

Bethe approach study of the mixed spin-1/2 and spin-5/2 Ising system in the presence of an applied magnetic field

M. Karimou¹, R.A. Yessoufou^{1,2*}, T.D. Oke^{1,2}, A. Kpadonou^{1,3}, F. Hontinfinde^{1,2}

¹ Institute of Mathematics and Physical Sciences (IMSP), Republic of Benin

² Department of Physics, University of Abomey-Calavi, Republic of Benin

³ University of Natitingou, École Normale Supérieure, Republic of Benin

Received January 18, 2016, in final form May 13, 2016

The mixed spin-1/2 and spin-5/2 Ising model is investigated on the Bethe lattice in the presence of a magnetic field h via the recursion relations method. A ground-state phase diagram is constructed which may be needful to explore important regions of the temperature phase diagrams of a model. The order-parameters, the corresponding response functions and internal energy are thoroughly investigated in order to typify the nature of the phase transition and to get the corresponding temperatures. So, in the absence of the magnetic field, the temperature phase diagrams are displayed in the case of an equal crystal-field on the $(k_B T/|J|, D/|J|)$ plane when $q = 3, 4, 5$ and 6 . The model only exhibits the second-order phase transition for appropriate values of physical parameters of a model.

Key words: *magnetic systems, thermal variations, phase diagrams, magnetic field, second-order transition*

PACS: 05.50.+q, 05.70.Ce, 64.60.Cn, 75.10.Hk, 75.30.Gw

1. Introduction

Over the last five decades, the Ising model has been one of the most largely used models to describe critical behaviors of several systems in nature. Lately, numerous extensions have been made in the spin- $\frac{1}{2}$ Ising model to describe a wide variety of systems. For example, the models consisting of mixed spins with different magnitudes are interesting extensions, forming the so-called mixed-spin Ising class [1, 2]. Beyond that, magnetic materials have several important technological applications: they find wide use in information storage devices, microwaves communication systems, electric power transformers and dynamo, and high-fidelity speakers [3–6]. Thus, in response to an increasing demand placed on the performance of magnetic solids, there has been a surge of interest in molecular-based magnetic materials [7–10]. Indeed, the discovery of these materials [11] has been one of the advances in modern magnetism. Many magnetic materials have two types of magnetic atoms regularly alternating which exhibit ferrimagnetism. In this context, a good description of their physical properties is given by means of mixed-spin configurations. The interest in studying magnetic properties of these materials is due to their reduced translational symmetry rather than to their single-spin counterparts, since they consist of two interpenetrating sublattices. Thus, ferrimagnetic materials are of great interest due to their possible technological applications and from a fundamental point of view. These materials are modelled using mixed-spin Ising models that can be built up by infinite combinations of different spins.

In literature there exist many studies on mixed-spin Ising systems which intend to clarify the magnetic properties of magnetic systems. In this regard, there has been great interest in the study of magnetic properties of the systems formed by two sublattices with different spins and crystal-field interactions [12]. Theoretically, such systems have been widely analysed using several numerical approaches,

*E-mail: yesradca@yahoo.fr, olorire2012@gmail.com

e.g., effective-field theory [13–18], mean-field approximation [19–23], renormalization-group technique [24, 25], numerical simulations based on Monte-Carlo [26–30] and exact recursion equations [31–38]. A somewhat newer interest is to extend such investigations into a more general mixed-spin Ising model with one constituent spin- $\frac{1}{2}$ and the other constituent spin- $\frac{5}{2}$. To this end, Deriven *et al.* [18] used an effective-field theory with correlation to study the same model and got interesting results. Recently, Guo *et al.* [17] studied the thermal entanglement of the same model by means of the concept of negativity and also got interesting results concerning the effects of the magnetic field on the entanglement.

In the present paper, we use the exact recursion equations technique to examine the magnetic properties of the mixed spin- $\frac{1}{2}$ and spin- $\frac{5}{2}$ Ising model with equal crystal-field on the Bethe lattice in the presence of a longitudinal magnetic field. The aim of this work is to investigate the effect of the crystal-field and the magnetic field on the physical magnetic properties of the model.

The remainder of this paper is arranged as follows. In section 2, the description of the model on the Bethe lattice is clarified. Furthermore, the order-parameters, the corresponding response functions and the internal energy are expressed in terms of recursion relations. In the next section, some definitions of the critical temperature of the model are explained. In section 4, we present some illustrations and discuss in detail the numerical results. We finally conclude in the last section.

2. Description of the model on the Bethe lattice

The mixed spins system on the Bethe lattice is shown in figure 1. We consider the mixed spin- $\frac{1}{2}$ and spin- $\frac{5}{2}$ system consisting of two sublattices A and B. The sites of sublattice A are occupied by atoms of spins S_i , where $S_i = \pm \frac{1}{2}$. Those of the sublattice B are occupied by atoms of spins σ_j , where $\sigma_j = \pm \frac{5}{2}, \pm \frac{3}{2}, \pm \frac{1}{2}$. In our case, the Bethe lattice is arranged in such a way that the central spin is spin- $\frac{1}{2}$ and the next generation spin is spin- $\frac{5}{2}$ and so on to infinity. Thus, the Ising Hamiltonian of such a model on the Bethe lattice may be written as:

$$H = -J \sum_{\langle i,j \rangle} \sigma_j S_i - D \sum_j \sigma_j^2 - h \left(\sum_i S_i + \sum_j \sigma_j \right); \quad (2.1)$$

$J < 0$ is the bilinear exchange coupling interaction strength. D and h are, respectively, the single-ion anisotropy or the crystal-field and the longitudinal magnetic field acting on the spins of the model.

In order to formulate the problem on the Bethe lattice, the partition function is the main ingredient

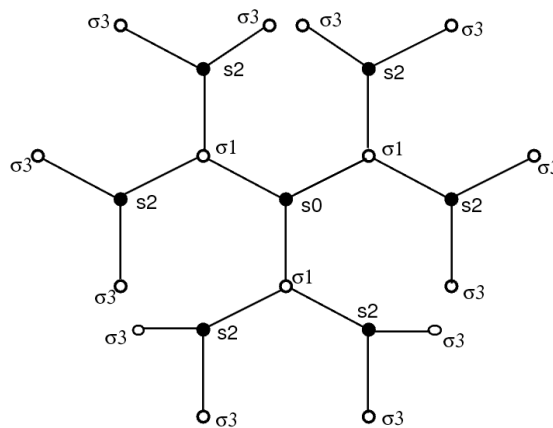


Figure 1. The mixed spin Ising model consisting of two different magnetic atoms with spins values $s_i = \frac{1}{2}$ and $\sigma_j = \frac{5}{2}$, respectively, defined on the Bethe lattice with coordination number $q = 3$.

which is given as:

$$Z = \sum \exp \left\{ \beta \left[J \sum_{\langle i,j \rangle} \sigma_j S_i + D \sum_j \sigma_j^2 + h \left(\sum_i S_i + \sum_j \sigma_j \right) \right] \right\}. \quad (2.2)$$

If the Bethe lattice is cut at the central spin S_0 , it splits into q disconnected pieces. Thus, the partition function on the Bethe lattice can be written as:

$$Z = \sum_{S_0} \exp [\beta(hS_0)] g_n^q(S_0), \quad (2.3)$$

where S_0 is the central spin value of the lattice, $g_n(S_0)$ is the partition function of an individual branch and the suffix n represents the fact that the sub-tree has n shells, i.e., n steps from the root to the boundary sites. If we continue to cut the Bethe lattice on the sites σ_1 and S_2 which are respectively the nearest and the next-nearest of the central spin S_0 , we can obtain the recurrence relations for $g_n(S_0)$ and $g_{n-1}(\sigma_1)$ as:

$$g_n(S_0) = \sum_{\{\sigma_1\}} \exp [\beta(JS_0\sigma_1 + D\sigma_1^2 + h\sigma_1)] [g_{n-1}(\sigma_1)]^{q-1}, \quad (2.4)$$

$$g_{n-1}(\sigma_1) = \sum_{\{S_2\}} \exp [\beta(JS_2\sigma_1 + hS_2)] [g_{n-2}(S_2)]^{q-1}. \quad (2.5)$$

Now, we explicitly calculate some $g_n(S_0)$ and $g_{n-1}(\sigma_1)$ as follows:

$$\begin{aligned} g_n\left(\pm\frac{1}{2}\right) &= \sum_{\{\sigma_1\}} \exp \left[\beta \left(\pm\frac{J}{2}\sigma_1 + D\sigma_1^2 + h\sigma_1 \right) \right] [g_{n-1}(\sigma_1)]^{q-1} \\ &= \exp \left[\beta \left(\pm\frac{5J}{4} + \frac{25}{4}D + \frac{5}{2}h \right) \right] \left[g_{n-1}\left(\frac{5}{2}\right) \right]^{q-1} + \exp \left[\beta \left(\mp\frac{5J}{4} + \frac{25}{4}D - \frac{5}{2}h \right) \right] \left[g_{n-1}\left(-\frac{5}{2}\right) \right]^{q-1} \\ &\quad + \exp \left[\beta \left(\pm\frac{3J}{4} + \frac{9}{4}D + \frac{3}{2}h \right) \right] \left[g_{n-1}\left(\frac{3}{2}\right) \right]^{q-1} + \exp \left[\beta \left(\mp\frac{3J}{4} + \frac{9}{4}D - \frac{3}{2}h \right) \right] \left[g_{n-1}\left(-\frac{3}{2}\right) \right]^{q-1} \\ &\quad + \exp \left[\beta \left(\pm\frac{J}{4} + \frac{1}{4}D + \frac{1}{2}h \right) \right] \left[g_{n-1}\left(\frac{1}{2}\right) \right]^{q-1} + \exp \left[\beta \left(\mp\frac{J}{4} + \frac{1}{4}D - \frac{1}{2}h \right) \right] \left[g_{n-1}\left(-\frac{1}{2}\right) \right]^{q-1}, \end{aligned} \quad (2.6)$$

$$\begin{aligned} g_{n-1}\left(\pm\frac{5}{2}\right) &= \sum_{\{S_2\}} \exp \left[\beta \left(\pm\frac{5J}{2}S_2 + hS_2 \right) \right] [g_{n-2}(S_2)]^{q-1} \\ &= \exp \left[\beta \left(\pm\frac{5J}{4} + \frac{h}{2} \right) \right] \left[g_{n-2}\left(\frac{1}{2}\right) \right]^{q-1} + \exp \left[\beta \left(\mp\frac{5J}{4} - \frac{h}{2} \right) \right] \left[g_{n-2}\left(-\frac{1}{2}\right) \right]^{q-1}, \end{aligned} \quad (2.7)$$

$$\begin{aligned} g_{n-1}\left(\pm\frac{3}{2}\right) &= \sum_{\{S_2\}} \exp \left[\beta \left(\pm\frac{3J}{2}S_2 + hS_2 \right) \right] [g_{n-2}(S_2)]^{q-1} \\ &= \exp \left[\beta \left(\pm\frac{3J}{4} + \frac{h}{2} \right) \right] \left[g_{n-2}\left(\frac{1}{2}\right) \right]^{q-1} + \exp \left[\beta \left(\mp\frac{3J}{4} - \frac{h}{2} \right) \right] \left[g_{n-2}\left(-\frac{1}{2}\right) \right]^{q-1}, \end{aligned} \quad (2.8)$$

$$\begin{aligned} g_{n-1}\left(\pm\frac{1}{2}\right) &= \sum_{\{S_2\}} \exp \left[\beta \left(\pm\frac{J}{2}S_2 + hS_2 \right) \right] [g_{n-2}(S_2)]^{q-1} \\ &= \exp \left[\beta \left(\pm\frac{J}{4} + \frac{h}{2} \right) \right] \left[g_{n-2}\left(\frac{1}{2}\right) \right]^{q-1} + \exp \left[\beta \left(\mp\frac{J}{4} - \frac{h}{2} \right) \right] \left[g_{n-2}\left(-\frac{1}{2}\right) \right]^{q-1}. \end{aligned} \quad (2.9)$$

After calculating all the $g_n(S_0)$ and $g_{n-1}(\sigma_1)$, we can define the recursion relations for the spin- $\frac{1}{2}$ as:

$$Z_n = \frac{g_n\left(\frac{1}{2}\right)}{g_n\left(-\frac{1}{2}\right)},$$

and for the spin- $\frac{5}{2}$ as:

$$\begin{aligned} A_{n-1} &= \frac{g_{n-1}(\frac{5}{2})}{g_{n-1}(-\frac{1}{2})}, & B_{n-1} &= \frac{g_{n-1}(-\frac{5}{2})}{g_{n-1}(-\frac{1}{2})}, & C_{n-1} &= \frac{g_{n-1}(\frac{3}{2})}{g_{n-1}(-\frac{1}{2})}, \\ D_{n-1} &= \frac{g_{n-1}(-\frac{3}{2})}{g_{n-1}(-\frac{1}{2})}, & E_{n-1} &= \frac{g_{n-1}(\frac{1}{2})}{g_{n-1}(-\frac{1}{2})}. \end{aligned} \quad (2.10)$$

To investigate our model, we define two order-parameters, the magnetization M and the corresponding quadrupolar moment Q . For the sublattice A, the sublattice magnetization M_A is defined by:

$$M_A = Z_A^{-1} \sum_{\{S_0\}} S_0 \exp(\beta h S_0) g_n^q(S_0). \quad (2.11)$$

After some mathematical manipulations, the sublattice magnetization M_A is explicitly given by:

$$M_A = \frac{\exp\left(\frac{\beta h}{2}\right) Z_n^q - \exp\left(-\frac{\beta h}{2}\right)}{2 \left[\exp\left(\frac{\beta h}{2}\right) Z_n^q + \exp\left(-\frac{\beta h}{2}\right) \right]}. \quad (2.12)$$

In the same way, we also calculate the two order-parameters for the sublattice B as follows:

$$M_B = \frac{M'_B}{M_B^0}, \quad Q_B = \frac{Q'_B}{Q_B^0},$$

where:

$$\begin{aligned} M'_B &= 5 \exp\left(\frac{25}{4}\beta D\right) \left[\exp\left(\frac{5}{2}\beta h\right) A_{n-1}^q - \exp\left(-\frac{5}{2}\beta h\right) B_{n-1}^q \right] + 3 \exp\left(\frac{9}{4}\beta D\right) \left[\exp\left(\frac{3}{2}\beta h\right) C_{n-1}^q \right. \\ &\quad \left. - \exp\left(-\frac{3}{2}\beta h\right) D_{n-1}^q \right] + \exp\left(\frac{1}{4}\beta D\right) \left[\exp\left(\frac{1}{2}\beta h\right) E_{n-1}^q - \exp\left(-\frac{1}{2}\beta h\right) \right], \end{aligned} \quad (2.13)$$

$$\begin{aligned} M_B^0 &= 2 \exp\left(\frac{25}{4}\beta D\right) \left[\exp\left(\frac{5}{2}\beta h\right) A_{n-1}^q + \exp\left(-\frac{5}{2}\beta h\right) B_{n-1}^q \right] + 2 \exp\left(\frac{9}{4}\beta D\right) \left[\exp\left(\frac{3}{2}\beta h\right) C_{n-1}^q \right. \\ &\quad \left. + \exp\left(-\frac{3}{2}\beta h\right) D_{n-1}^q \right] + 2 \exp\left(\frac{1}{4}\beta D\right) \left[\exp\left(\frac{1}{2}\beta h\right) E_{n-1}^q + \exp\left(-\frac{1}{2}\beta h\right) \right], \end{aligned} \quad (2.14)$$

$$\begin{aligned} Q'_B &= 25 \exp\left(\frac{25}{4}\beta D\right) \left[\exp\left(\frac{5}{2}\beta h\right) A_{n-1}^q + \exp\left(-\frac{5}{2}\beta h\right) B_{n-1}^q \right] + 9 \exp\left(\frac{9}{4}\beta D\right) \left[\exp\left(\frac{3}{2}\beta h\right) C_{n-1}^q \right. \\ &\quad \left. + \exp\left(-\frac{3}{2}\beta h\right) D_{n-1}^q \right] + \exp\left(\frac{1}{4}\beta D\right) \left[\exp\left(\frac{1}{2}\beta h\right) E_{n-1}^q + \exp\left(-\frac{1}{2}\beta h\right) \right], \end{aligned} \quad (2.15)$$

$$\begin{aligned} Q_B^0 &= 4 \exp\left(\frac{25}{4}\beta D\right) \left[\exp\left(\frac{5}{2}\beta h\right) A_{n-1}^q + \exp\left(-\frac{5}{2}\beta h\right) B_{n-1}^q \right] + 4 \exp\left(\frac{9}{4}\beta D\right) \left[\exp\left(\frac{3}{2}\beta h\right) C_{n-1}^q \right. \\ &\quad \left. + \exp\left(-\frac{3}{2}\beta h\right) D_{n-1}^q \right] + 4 \exp\left(\frac{1}{4}\beta D\right) \left[\exp\left(\frac{1}{2}\beta h\right) E_{n-1}^q + \exp\left(-\frac{1}{2}\beta h\right) \right]. \end{aligned} \quad (2.16)$$

In order to determine the compensation temperature, one has to define the global magnetization M_T of the model which is given by:

$$M_T = \frac{M_A + M_B}{2}. \quad (2.17)$$

To really study the model in detail and single out the effect of the crystal-field and of the applied magnetic field on the magnetic properties of the model, we have also examined the thermal variations of the

response functions, i.e., the susceptibilities, the specific heat and the internal energy defined respectively by:

$$\chi_{\text{Total}} = \chi_A + \chi_B = \left(\frac{\partial M_A}{\partial h} \right)_{h=0} + \left(\frac{\partial M_B}{\partial h} \right)_{h=0}, \quad (2.18)$$

$$C = -\beta^2 \frac{\partial^2 (-\beta F')}{\partial \beta^2}, \quad (2.19)$$

$$\frac{U}{N|J|} = -k_B T^2 \frac{\partial}{\partial T} \left(\frac{F'}{k_B T} \right), \quad (2.20)$$

where F' is the free energy of the model.

3. Definition of the critical temperature

The Curie temperature or the second-order transition temperature T_c is the temperature at which both sublattice magnetizations and the global magnetization continuously go to zero. T_c separates the ordered ferrimagnetic phase (F) from the disordered paramagnetic phase (P). At T_c , one can obtain explicit expressions of the recursion relations as follows:

for the spin- $\frac{1}{2}$,

$$Z_n = 1, \quad (3.1)$$

and for the spin- $\frac{5}{2}$,

$$A_{n-1} = B_{n-1} = \frac{\cosh\left(\frac{5\beta J}{4}\right)}{\cosh\left(\frac{\beta J}{4}\right)}, \quad C_{n-1} = D_{n-1} = \frac{\cosh\left(\frac{3\beta J}{4}\right)}{\cosh\left(\frac{\beta J}{4}\right)}, \quad E_{n-1} = 1. \quad (3.2)$$

In addition to the thermal variations of the order-parameters and the global magnetization of the model, we also calculate and analyze the free energy F' of the model in order to identify the first-order transition temperature T_t . Thus, using the definition of the free energy $F' = -k_B T \ln(Z)$ in the thermodynamic limit ($n \rightarrow \infty$) and in order to introduce the recursion relations, we can rewrite the free energy as:

$$F'/J = -\frac{1}{\beta'} \left[\frac{q-1}{2-q} \ln F_1 + \frac{1}{2-q} \ln F_2 + \ln F_3 \right], \quad (3.3)$$

where $\beta' = \beta J$, $F_1 = g_{n-1}(-1/2)/g_n^{q-1}(-1/2)$, $F_2 = g_n(-1/2)/g_{n-1}^{q-1}(-1/2)$ and $F_3 = Z/g_n^q(-1/2)$.

After some mathematical manipulations, the free energy expression in terms of recursion relations is explicitly given by:

$$\begin{aligned} F'/J = & -\frac{1}{\beta'} \left(\frac{q-1}{2-q} \ln \left\{ \exp \left[\beta \left(-\frac{J}{4} + \frac{h}{2} \right) \right] Z_n^{q-1} + \exp \left[\beta \left(\frac{J}{4} - \frac{h}{2} \right) \right] \right\} \right) \\ & - \frac{1}{\beta'} \left\{ \ln \left[\exp \left(\beta \frac{h}{2} \right) Z_n^q + \exp \left(-\beta \frac{h}{2} \right) \right] \right\} \\ & - \frac{1}{\beta'} \left(\frac{1}{2-q} \ln \left\{ \exp \left[\beta \left(-\frac{5J}{4} + \frac{25D}{4} + \frac{5h}{2} \right) \right] A_{n-1}^{q-1} + \exp \left[\beta \left(\frac{5J}{4} + \frac{25D}{4} - \frac{5h}{2} \right) \right] B_{n-1}^{q-1} \right. \right. \\ & + \exp \left[\beta \left(-\frac{3J}{4} + \frac{9D}{4} + \frac{3h}{2} \right) \right] C_{n-1}^{q-1} + \exp \left[\beta \left(\frac{3J}{4} + \frac{9D}{4} - \frac{3h}{2} \right) \right] D_{n-1}^{q-1} \\ & \left. \left. + \exp \left[\beta \left(-\frac{J}{4} + \frac{D}{4} + \frac{h}{2} \right) \right] E_{n-1}^{q-1} + \exp \left[\beta \left(\frac{J}{4} + \frac{D}{4} - \frac{h}{2} \right) \right] \right\} \right). \end{aligned} \quad (3.4)$$

We also investigate the compensation temperature T_{comp} at which the global magnetization vanishes while both sublattice magnetizations cancel each other. T_{comp} is found by locating the crossing point between the absolute values of sublattice magnetizations, i.e.,

$$|M_A(T_{\text{comp}})| = |M_B(T_{\text{comp}})|. \quad (3.5)$$

Considering different definitions of the critical temperature, we can now investigate the thermal variations of the calculated thermodynamical quantities of interest and display the temperature phase diagrams of the model for $q = 3, 4, 5$ and 6.

4. Numerical results and discussions

In this section, we present and discuss the results we obtained for the thermal variations of the order-parameters, the response functions, the internal energy and the temperature phase diagrams of the model. We begin discussions with the ground-state phase diagram which is necessary for understanding the obtained temperature phase diagrams.

4.1. Ground-state phase diagram

Before presenting the numerical results for the temperature dependence of magnetic properties of the model, we first investigate the ground-state phase diagram. The ground-state structure of the model can be represented by comparing the values of the energy H_0 for different spin configurations which can be expressed as:

$$H_0 = S\sigma - \frac{1}{q|J|} [D\sigma^2 + h(S + \sigma)]. \quad (4.1)$$

We only get eleven possible pairs of spins. Computational calculations of the corresponding energies in the $(h/q|J|, D/q|J|)$ plane yields the ground-state phase diagram displayed in figure 2. This diagram shows some interesting features of the model, in particular, the existence of eight multicritical points

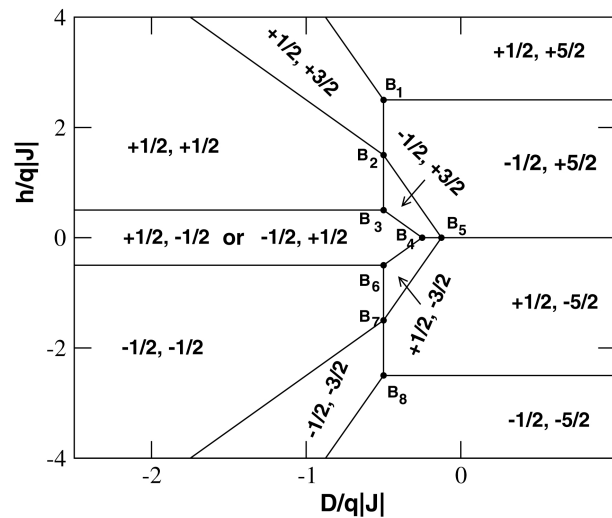


Figure 2. Ground-state phase diagram of the mixed spin- $\frac{1}{2}$ and spin- $\frac{5}{2}$ Ising ferrimagnetic model with the same crystal-field D for the two sublattices in the $(h/q|J|, D/q|J|)$ plane. There exist eleven stable phases. Along the $D/q|J|$ -axis and for all values of q , two hybrid phases may appear at the multicritical points B_4 and B_5 .

(B_1, B_2, \dots, B_8) and coexistence lines where the spin pair energy of some phases is the same. In the absence of the magnetic field, for all values of q and $D/q|J|$, M_B shows five saturation values whereas for M_A , $\pm \frac{1}{2}$ is the only saturation value. Thus, we get the ferrimagnetic phases $F(\pm \frac{1}{2}, \mp \frac{5}{2})$, $F(\pm \frac{1}{2}, \mp \frac{3}{2})$, $F(\pm \frac{1}{2}, \mp \frac{1}{2})$ and at the borders of these phases, two hybrid phases: $F(\pm \frac{1}{2}, \mp 1)$, $F(\pm \frac{1}{2}, \mp 2)$ at the multicritical points B_4 and B_5 , respectively. These hybrid phases should correspond to cases where the sublattice B is half-half covered by spins of the two neighboring phases. It is important to indicate that the ground-state phase diagram is very useful because it helps to check the reliability of the theoretical results and to classify different phase domains of the model for the temperature dependence phase diagrams.

4.2. Thermal variations of the order-parameters, the response functions and the internal energy

As it is explained above, thermal variations of the order-parameters, the response functions and the internal energy for the present model were calculated in terms of recursion relations. Thermal variations of the order-parameters are crucial in obtaining the temperature dependence phase diagrams of the model. Thus, when the magnetization curves go to zero continuously separating the ferrimagnetic phase from the paramagnetic phase, one gets the second-order phase transition or Curie temperature, i.e., the temperature at which magnetizations become zero. In the case of a jump in the magnetization curves

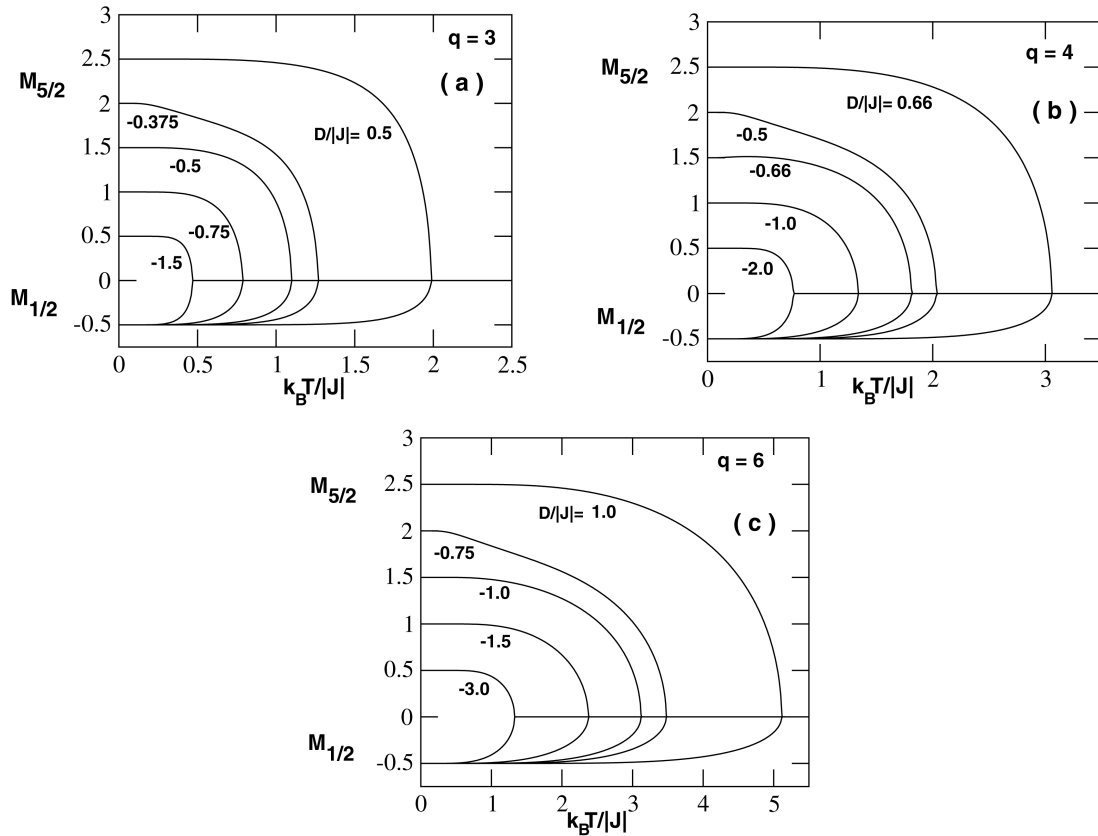


Figure 3. Sublattice magnetizations of the model as functions of the reduced temperature $k_B T / |J|$ when $q = 3, 4$ and 6 for various values of the crystal-field interactions $D/|J|$. Panel (a): Curves are displayed for $q = 3$ and selected values of $D/|J|$ indicated on the curves. Panel (b): curves are displayed for $q = 4$ and selected values of $D/|J|$ indicated on the curves. Panel (c): curves are displayed for $q = 6$ and selected values of $D/|J|$ indicated on the curves. For all values of q , the sublattice magnetization curves are all continuous.

followed by a discontinuity of the first derivative of the free-energy F' , one gets a first-order transition temperature. Besides these two temperatures, there is another temperature referred to as compensation temperature defined as the temperature where the global magnetization becomes zero prior to the critical temperature. Therefore, in order to identify transitions and compensation lines, one should study the thermal behaviors of the considered thermodynamical quantities of the model. Now, we present some results on the thermal behaviors of the order-parameters, the response functions and the internal energy in the absence of the magnetic field h when $q = 3, 4$ and 6 .

Figure 3 displays some thermal variations of the sublattice magnetizations $M_{1/2}$ and $M_{5/2}$ when $q = 3, 4$ and 6 for selected values of the crystal-field $D/|J|$. From panels (a) to (c), we have depicted the thermal behaviors of sublattice magnetizations $M_{1/2}$ and $M_{5/2}$ as functions of the temperature for selected values of $D/|J|$ when $q = 3, 4$ and 6 . The results are in perfect agreement with the ground-state phase diagram concerning the saturation values. Indeed, $M_{1/2}$ increases from its unique saturation value $\pm \frac{1}{2}$ with increasing temperature whereas $M_{5/2}$ shows five saturation values. The behaviors of the sublattice magnetizations $M_{1/2}$ and $M_{5/2}$ are quite similar. We notice that all the curves are continuous and the Curie temperature T_c at which both magnetizations curves go to zero increases with the strength of the crystal-field $D/|J|$ and the coordination number q . Moreover, by comparing figure 3 to figure 4 of [18], the sublattice magnetizations show similar thermal variations.

To explain in detail the results obtained in figure 3, we have investigated the thermal variations of order-parameters, the corresponding response functions and the internal energy.

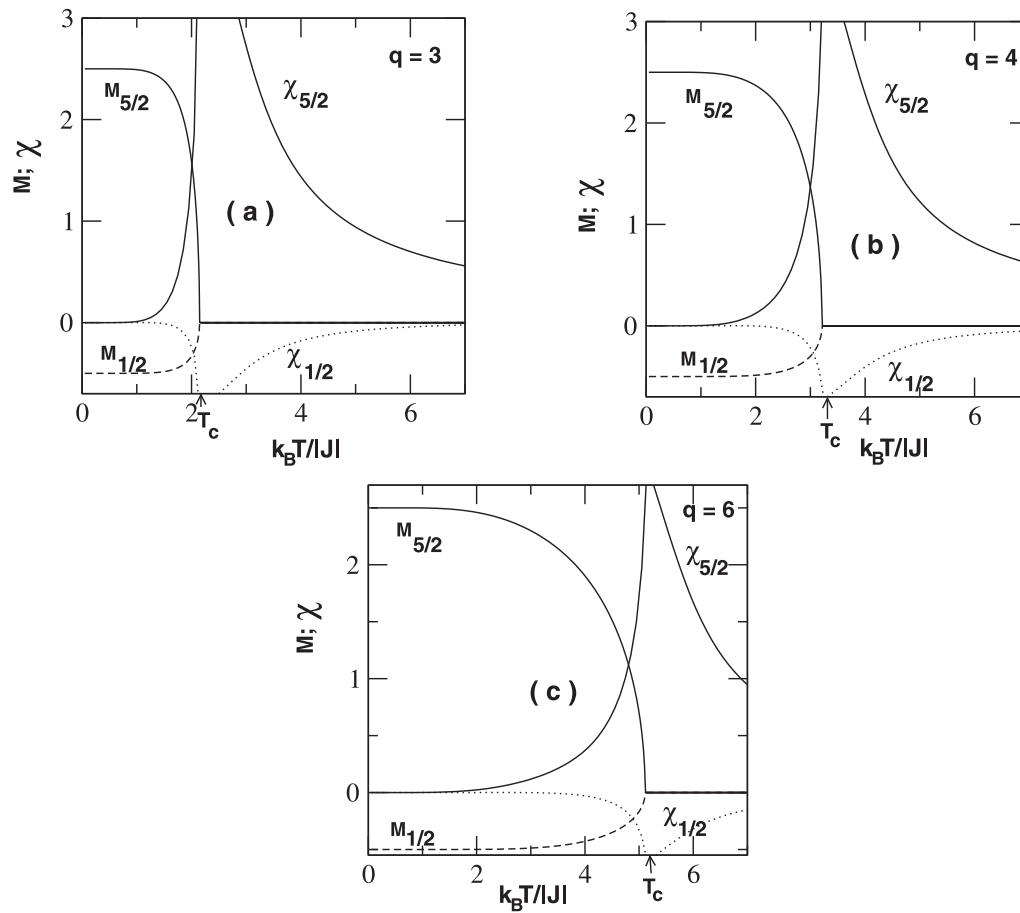


Figure 4. Thermal variations of sublattice magnetizations and corresponding susceptibilities are calculated for $q = 3, 4, 6$ and the reduced crystal-field $D/|J| = 1$ as shown from panel (a) to panel (c). Values of the physical parameters considered for the system are indicated in different panels. T_c indicates the second-order temperature.

Thus, on the one hand, as shown in figure 4, we have displayed the thermal behaviors of the sublattice magnetizations and corresponding susceptibilities when $q = 3, 4, 6$ and $D/|J| = 1$. In this figure, one can notice that the model only exhibits the second-order phase transition, and the transition temperature T_c at which the transition occurs increases with an increasing coordination number q . Here, T_c separates the ferrimagnetic phase $F(\pm\frac{1}{2}, \mp\frac{5}{2})$ from the paramagnetic phase (P) and $T_c/|J| = 2.1724$ (respectively $T_c/|J| = 3.2575$ and 5.1398) for $q = 3$ (respectively for $q = 4$ and 6). Also, one remarks that for $T \rightarrow T_c$, $\chi_{1/2} \rightarrow -\infty$ whereas $\chi_{5/2} \rightarrow +\infty$. For $T > T_c$, the susceptibility $\chi_{1/2}$ rapidly increases whereas the susceptibility $\chi_{5/2}$ rapidly decreases when the temperature increases and is very far from the Curie temperature T_c , $\chi_{1/2} \rightarrow 0$ and $\chi_{5/2} \rightarrow 0$.

On the other hand, to really confirm that the model only exhibits the second-order transition for all values of q , we have plotted in figure 5 the temperature dependence variations of the specific heat and the internal energy for various values of the crystal-field as indicated in the figure. Both the specific heat and the internal energy rapidly increase with an increasing temperature and make a peak without jump discontinuities at the same T_c . By increasing the strength of the crystal-field and the coordination number, the T_c at which the transition occurs, increases and this is easily observed by comparing the results from different panels of figure 5. The results obtained in this figure also confirm that the model only presents second-order transition for all values of the coordination number q .

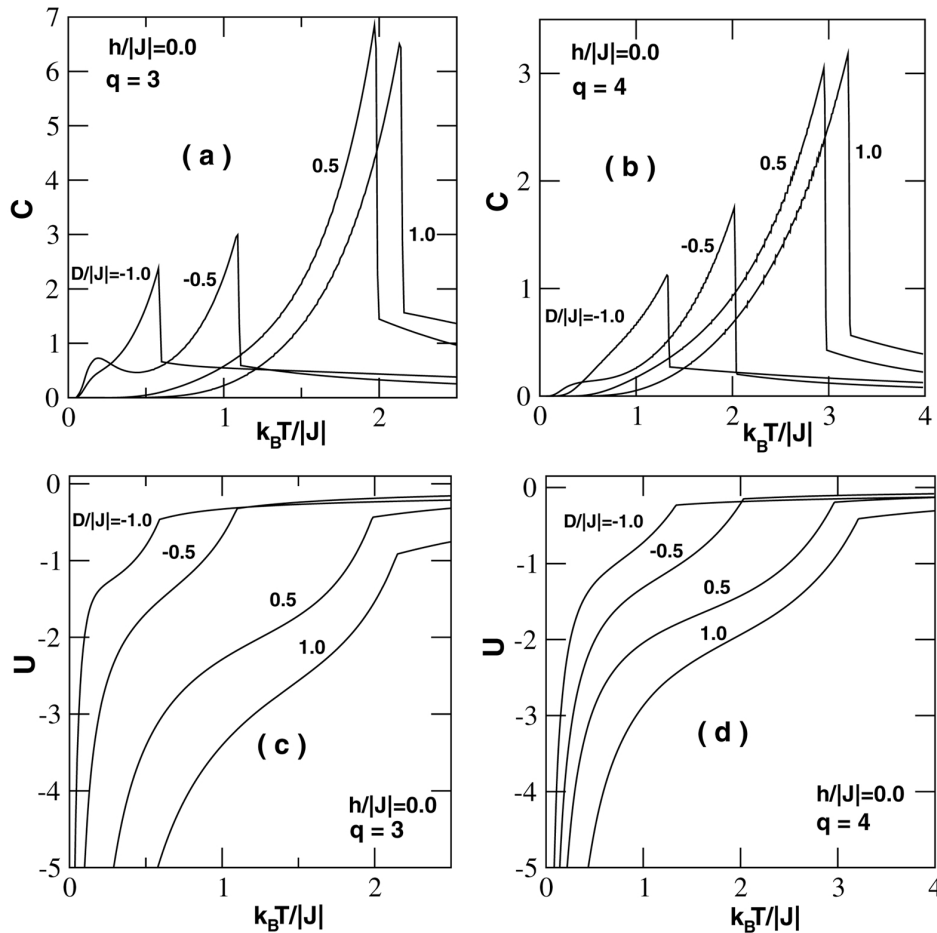


Figure 5. Thermal variations of the specific heat and internal energy are calculated for $q = 3, 4$ and selected values of the crystal-field $D/|J|$ as shown in the figures from panel (a) to panel (d). Values of the physical parameters considered for the system are indicated in different panels. Analysis of different panels of this figure shows that the model only exhibits a second-order transition.

Let us now discuss the thermal variations of sublattice magnetizations, the corresponding response functions and the internal energy of the system in the presence of a longitudinal magnetic field h .

Figure 6 expresses the effects of an applied magnetic field h on the magnetic properties of the model when $q = 3$ and $D/|J| = 1.0$ for selected values of $h/|J|$. From panel (a) to panel (b), the sublattice magnetizations and the global magnetization continuously fall from their saturation values to non-zero values when the temperature increases. The remaining values of magnetizations are more important when the value of the applied magnetic field $h/|J|$ increases. Thus, one can observe that the system does not present any transition when $h/|J| \neq 0$. It is important to indicate that in the case of $h/|J| = 0$, the model exhibits the second-order transition at a Curie temperature $T_c/|J| = 2.1724$, where the two sublattice magnetizations and the global magnetization continuously go to zero after falling from their saturation values at $T = 0$. In panels (c)–(e), we have displayed the temperature dependence of the total susceptibility χ_T , the specific heat C and the internal energy U . One can see from these panels that the response functions and the internal energy also indicate a second-order transition which occurs at the same $T_c/|J|$ as in the case

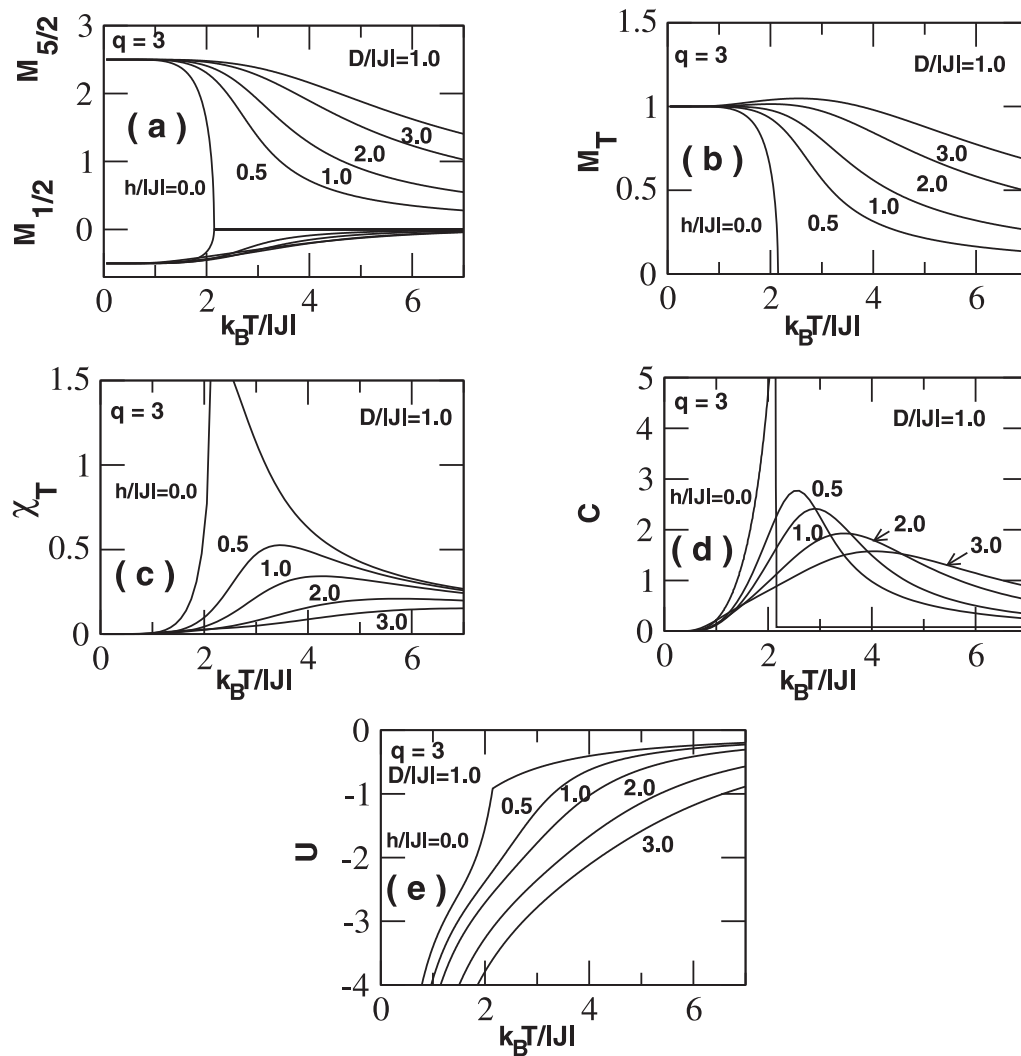


Figure 6. Thermal behaviors of the sublattice magnetizations, the global magnetization, the corresponding response functions and the internal energy of the model when $D/|J| = 1.0$ and $q = 3$ for selected values of the magnetic field $h/|J|$ as shown in different panels. From the analysis of different panels, one can conclude that the model only shows temperature phase transition when $h/|J| = 0$. For $h/|J| \neq 0$, the remaining magnetizations are more important when the value of the magnetic field $h/|J|$ increases.

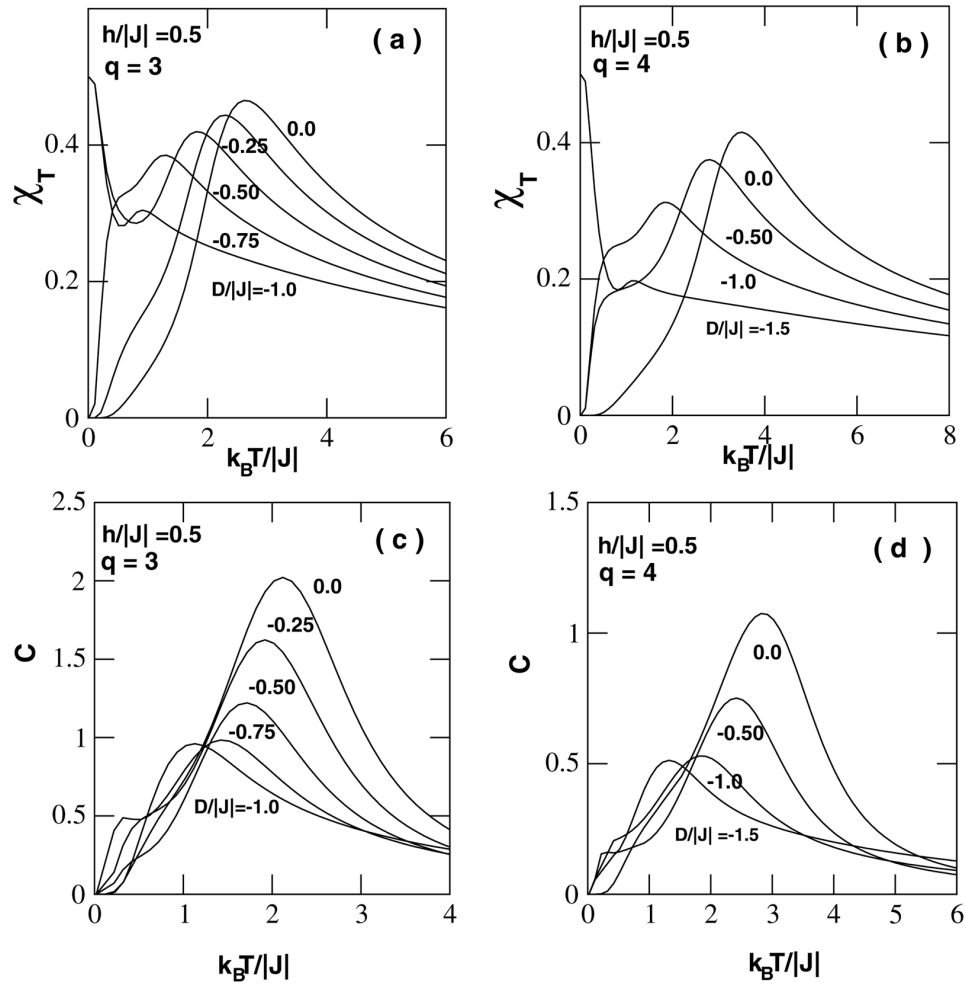


Figure 7. Temperature variations of the response functions of the model for selected values of the crystal-field $D/|J|$ as indicated on different curves illustrated when $h/|J| = 0.5$ and $q = 3, 4$.

of $h/|J| = 0$. For $h/|J| \neq 0$ and $T > T_c$, the response functions exhibit a maximum and the height of the maximum decreases when the value of the applied magnetic field increases.

To show the effect of $D/|J|$ on the system properties for $h/|J| \neq 0$, we have illustrated in figure 7 the thermal variations of the response functions for some values of the system parameters: $h/|J| = 0.5$; $q = 3, 4$ and varying $D/|J|$. Considering the different panels of figure 7, one observes that the response functions show interesting behaviors. Indeed, the two studied response functions globally show a maximum at a certain value of the temperature. This temperature increases with the coordination number and the strength of the crystal-field. It is important to mention that the height of the maximum of the two response functions also increases by increasing the strength of the crystal-field $D/|J|$ but the opposite holds when the coordination number q increases.

In order to investigate the low-temperature magnetic properties of the model, we plotted the sublattice magnetizations and the global magnetization at $k_B T/|J| = 0.05$ for selected values of the crystal-field as functions of the field h as shown in figure 8. In figure 8 (a) where $D/|J| = -1$ and $q = 3$, $M_{1/2}$ shows two step-like magnetization plateaus ($M_{1/2} = -\frac{1}{2}, \frac{1}{2}$) whereas $M_{5/2}$ and M_T respectively show three and four step-like magnetization plateaus ($M_{5/2} = \frac{1}{2}, \frac{3}{2}, \frac{5}{2}$) and ($M_T = 0, \frac{1}{2}, 1, \frac{3}{2}$). Also, from figure 8 (b) where $D/|J| = 0$ and $q = 3$, only $M_{1/2}$ and M_T present two step-like magnetization plateaus ($M_{1/2} = -\frac{1}{2}, \frac{1}{2}$) and ($M_T = 1, \frac{3}{2}$). The obtained results are consistent with the ground-state phase diagram displayed in figure 2. We also investigated the global magnetization as a function of the temperature and obtained some

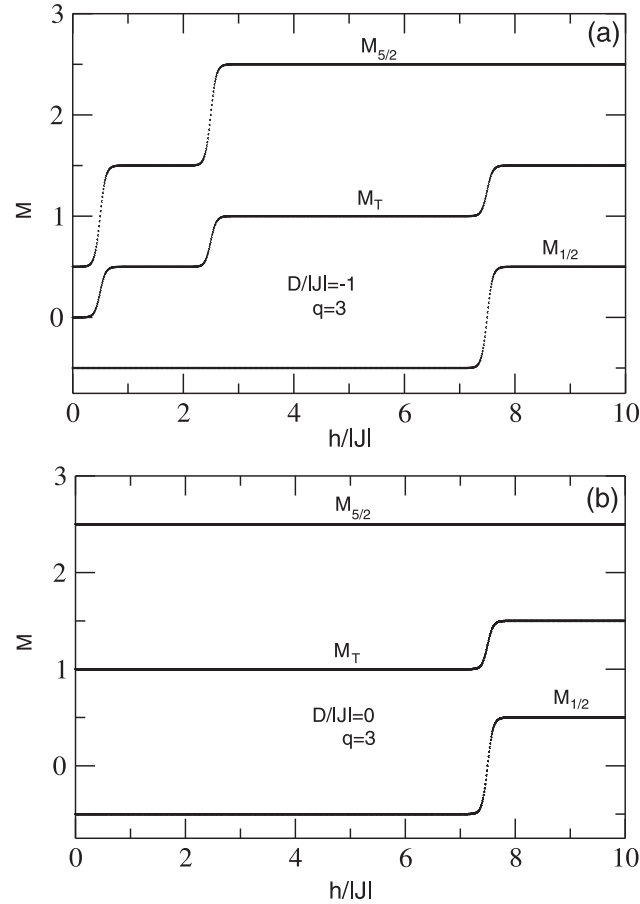


Figure 8. $M_{1/2}$, $M_{5/2}$ and M_T plotted as functions of the magnetic field h for selected values of the crystal-field when $q = 3$ as indicated in different panels.

compensation types of Ising model. Figure 9 shows temperature dependencies of the global magnetization M_T for selected values of the crystal-field when $q = 3$. As seen in figure 9, the model exhibits five types of compensation behaviors, namely Q-, R-, S-, L- and P-type compensation behaviors as classified in the extended Néel nomenclature [39].

4.3. Finite-temperature phase diagrams

Considering all the above calculations, we can illustrate the temperature phase diagrams of the model. So in figure 10, we have constructed the phase diagrams of the system in the $(D/|J|, k_B T/|J|)$ plane in the absence of a magnetic field h when $q = 3, 4, 5$ and 6 . In different phase diagrams, the solid line indicates the second-order transition line. Two filled triangles indicate two multicritical points B_4 and B_5 found in the ground-state phase diagram displayed in figure 2.

From this figure, some interesting properties of the system are singled out. Indeed, for all values of the coordination number q , from panel (a) to panel (d) where $q = 3, 4, 5$ and 6 , respectively, the transition lines are only of the second-order separating the ferrimagnetic phase (F) which is a mixture of five different ferrimagnetic phases from the paramagnetic phase (P) and become constant for $D/|J| < -q/4$. One can observe that: (1) When $D/|J| > -q/8$, the second-order phase transition turns from ferrimagnetic phase $F(\pm\frac{1}{2}, \mp\frac{5}{2})$ to a disordered paramagnetic phase P. (2) For $-q/4 < D/|J| < -q/8$, the second-order phase transition is from the ferrimagnetic $F(\pm\frac{1}{2}, \mp\frac{3}{2})$ to the paramagnetic phase P. (3) When $D/|J| < -q/4$, the second-order phase transition is from the ferrimagnetic phase $F(\pm\frac{1}{2}, \mp\frac{1}{2})$ to the paramagnetic phase

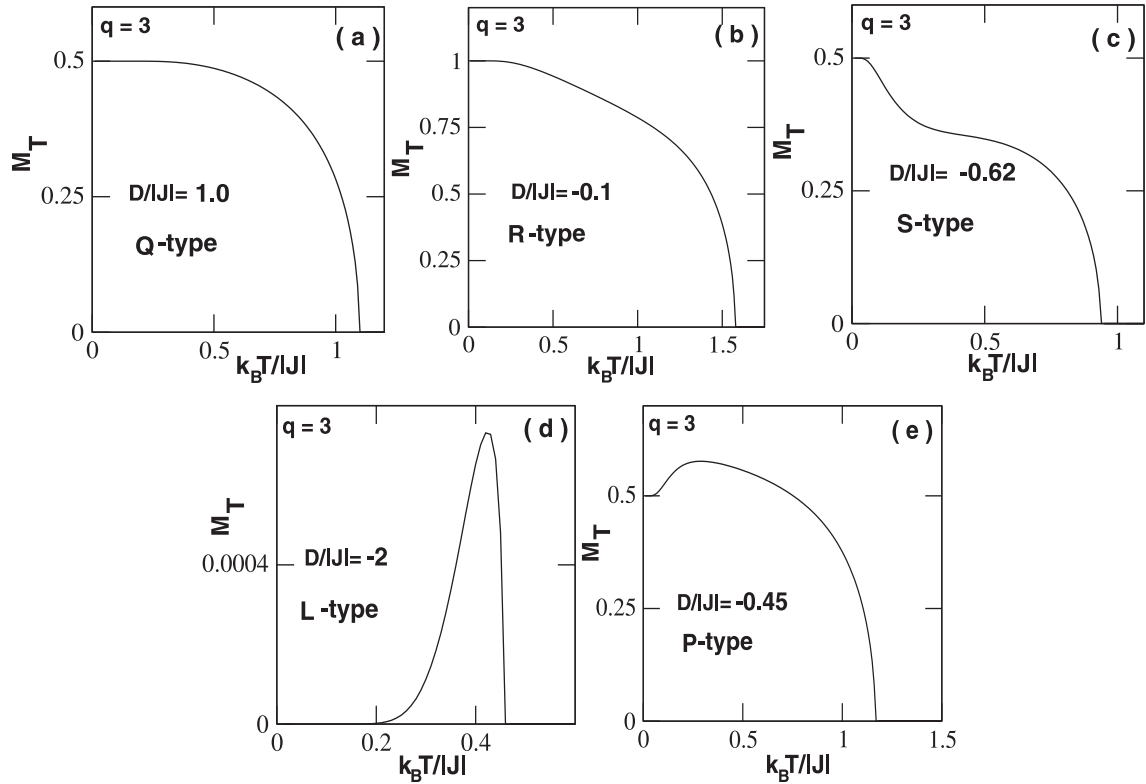


Figure 9. M_T as a function of the temperature for selected values of the crystal-field when $q = 3$ as indicated in different panels. The model shows the Q-, R-, S-, L- and P-types of compensation behaviors as classified in the extended Néel nomenclature.

P. (4) For $D/|J| = -q/8$ respectively $D/|J| = -q/4$, the second-order transition phase is from the hybrid phase $F(\pm\frac{1}{2}, \mp 2)$ respectively the hybrid phase $F(\pm\frac{1}{2}, \mp 1)$ to the paramagnetic phase P.

It is important to mention that figure 10 presents some resemblances concerning the second-order transition lines with figure 3 of [18]. Moreover, by increasing the value of the coordination number q , the ferrimagnetic domain F becomes important.

5. Conclusion

In this work, the study of the mixed spin- $\frac{1}{2}$ and spin- $\frac{5}{2}$ Ising ferrimagnetic model on the Bethe lattice in the presence of a longitudinal magnetic field is undertaken via exact recursion equations method. All the thermodynamical quantities of interest are calculated as functions of recursion relations.

The ground-state phase diagram of the model is displayed as shown in figure 2. From this phase diagram, we have found eleven existing and stable phases and along the $D/q|J|$ -axis, two particular hybrid phases appear at the two multicritical points B_4 and B_5 . The ground-state phase diagram is considered and used as a guide in obtaining different temperature phase diagrams. In the presence and in the absence of a longitudinal magnetic field h , we investigated thermal variations of sublattice magnetizations, global magnetization, the corresponding response functions and the internal energy as seen in figures 3–9. From these figures, the order-parameters in most cases showed a usual decay with thermal fluctuations. By using thermal behaviors of the considered order-parameters, and by analysing the corresponding response functions and the internal energy, the nature of different phase transitions encountered is identified. This enables us to construct and to discuss in detail different temperature dependence phase diagrams in the case of equal crystal-field interactions as shown in figure 10. The model shows rich physical properties, namely the second-order transition and multicritical points for all values of the crystal-field interactions and for all values of the coordination number q .

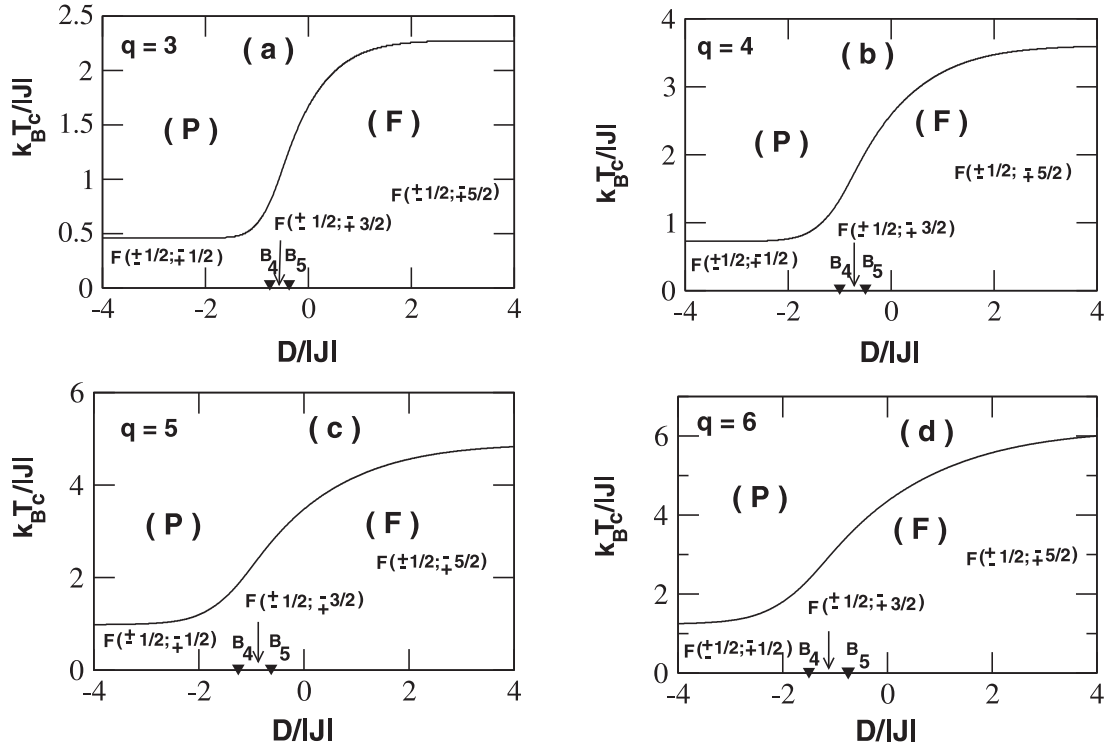


Figure 10. Temperature phase diagrams of the model in the $(D/|J|, k_B T_c/|J|)$ plane. The solid line indicates the second-order transition line. Panel (a): $q = 3$; panel (b): $q = 4$; panel (c): $q = 5$ and panel (d): $q = 6$. Here, the model only presents second-order transition for all values of q . The multicritical points B_4 and B_5 which respectively indicate the positions of the hybrid phases $F(\pm\frac{1}{2}, \mp 1)$ and $F(\pm\frac{1}{2}, \mp 2)$, respectively separate the ferrimagnetic phases $F(\pm\frac{1}{2}, \mp\frac{1}{2})$, $F(\pm\frac{1}{2}, \mp\frac{3}{2})$ and $F(\pm\frac{1}{2}, \mp\frac{5}{2})$.

Finally, it is useful to mention that different results found here are compared to those reported in some references, and some topological similarities are shown, especially with those found in [18] where the same model is investigated by means of the effective-field theory with correlation. However, during our investigation we have not found any compensation temperature.

References

1. Thompson C.J., Mathematical Statistical Mechanics, Princeton University Press, New Jersey, 1992.
2. Strečka J., Jaščur M., Acta Phys. Slovaca, 2015, **65**, 235, and references therein.
3. White R.M., Science, 1985, **229**, 11; doi:10.1126/science.229.4708.11.
4. Wood R., Understanding Magnetism, Tab Books Inc, Blue Ridge Summit, PA, 1988.
5. Köster E., J. Magn. Magn. Mater., 1993, **120**, 1; doi:10.1016/0304-8853(93)91274-B.
6. Lueck L.B., Gilson R.G., J. Magn. Magn. Mater., 1990, **88**, 227; doi:10.1016/S0304-8853(97)90032-9.
7. Molecular Magnetism: New Magnetic Materials, Itoh K., Kinoshita M. (Eds.), Kodansha, Tokyo, 2000.
8. Molecular Magnets. Recent Highlights, Linert W., Verdaguer M. (Eds.), Springer-Verlag, Wien, 2003.
9. Gatteschi D., Adv. Mater., 1994, **6**, 635; doi:10.1002/adma.19940060903.
10. Miller J.S., Epstein A.J., Chem. Eng. News, 1995, **73**, 30; doi:10.1021/cen-v073n040.p030.
11. Kahn O., Molecular Magnetism, VCH, New York, 1993.
12. Bobák A., Physica A, 1998, **258**, 140; doi:10.1016/S0378-4371(98)00233-7.
13. Benyoussef A., El Kenz A., Kaneyoshi T., J. Magn. Magn. Mater., 1994, **131**, 179; doi:10.1016/0304-8853(94)90026-4.
14. Bobák A., Jurčišin M., Physica A, 1997, **240**, 647; doi:10.1016/S0378-4371(97)00044-7.
15. De Oliveira D.C., Silva A.A.P., de Albuquerque D.F., de Arruda A.S., Physica A, 2007, **386**, 205; doi:10.1016/j.physa.2007.07.073.

16. Kaneyoshi T., Physica A, 1994, **205**, 677; doi:10.1016/0378-4371(94)90229-1.
17. Guo K.T., Xiang S.H., Xu H.Y., Li X.L., Quantum Inf. Process., 2014, **13**, 1511; doi:10.1007/s11128-014-0745-7.
18. Deviren B., Keskin M., Canko M.O., Physica A, 2009, **388**, 1835; doi:10.1016/j.physa.2009.01.032.
19. Da Cruz Filho J.S., Godoy M., de Arruda A.S., Physica A, 2013, **392**, 6247; doi:10.1016/j.physa.2013.08.007.
20. Miao H., Wei G., Geng J., J. Magn. Magn. Mater., 2009, **321**, 4139; doi:10.1016/j.jmmm.2009.08.018.
21. Mohamad H.K., Domashevskaya E.P., Klinskikh A.F., Physica A, 2009, **388**, 4713; doi:10.1016/j.physa.2009.08.014.
22. Mohamad H.K., Int. J. Adv. Res., 2014, **2**, No. 9, 442.
23. Kaneyoshi T., Chen J.C., J. Magn. Magn. Mater., 1991, **98**, 201; doi:10.1016/0304-8853(91)90444-F.
24. Quadros S.G.A., Salinas S.R., Physica A, 1994, **206**, 479; doi:10.1016/0378-4371(94)90319-0.
25. El Bouziani M., Gaye A., Jellal A., Physica A, 2013, **392**, 689; doi:10.1016/j.physa.2012.10.007.
26. Buendia G.M., Liendo J.A., J. Phys.: Condens. Matter, 1997, **9**, 5439; doi:10.1088/0953-8984/9/25/011.
27. Godoy M., Figueiredo W., Phys. Rev. E, 2002, **66**, 036131; doi:10.1103/PhysRevE.66.036131.
28. Cambui D.S., Arruda A.S., Godoy M., Int. J. Mod. Phys. C, 2012, **23**, 1240015; doi:10.1142/S0129183112400153.
29. Feraoun A., Zaim A., Kerouad M., Physica B, 2014, **445**, 74; doi:10.1016/j.physb.2014.03.071.
30. Žukovič M., Bobák A., J. Magn. Magn. Mater., 2010, **322**, 2868; doi:10.1016/j.jmmm.2010.04.043.
31. Yessoufou R.A., Bekhechi S., Hontinfinde F., Eur. Phys. J. B, 2011, **81**, 137; doi:10.1140/epjb/e2011-10825-7.
32. Kple J., Yessoufou R.A., Hontinfinde F., Afr. Rev. Phys., 2012, **7**, 319.
33. Yigit A., Albayrak E., Chinese Phys. B, 2012, **21**, 020511; doi:10.1088/1674-1056/21/2/020511.
34. Ekiz C., Phys. Lett. A, 2007, **367**, 483; doi:10.1016/j.physleta.2007.03.038.
35. Albayrak E., Yigit A., Phys. Lett. A, 2006, **353**, 121; doi:10.1016/j.physleta.2005.12.077.
36. Karimou M., Yessoufou R., Hontinfinde F., Int. J. Mod. Phys. B, 2015, **29**, 1550194; doi:10.1142/S0217979215501945.
37. Ekiz C., J. Magn. Magn. Mater., 2006, **307**, 139; doi:10.1016/j.jmmm.2006.03.059.
38. Ekiz C., Commun. Theor. Phys., 2009, **52**, 539; doi:10.1088/0253-6102/52/3/30.
39. Ekiz C., Strečka J., Jaščur M., Cent. Eur. J. Phys., 2009, **7**, 509; doi:10.2478/s11534-009-0043-7, and references therein.

Вивчення змішаної спин- $\frac{1}{2}$ і спин- $\frac{5}{2}$ моделі Ізінга на ґратці Бете під дією магнітного поля

М. Каріму¹, Р.А. Єссуфу^{1,2}, Т.Д. Оке^{1,2}, А. Кпандону^{1,3}, Ф. Онтінфінде^{1,2}

¹ Інститут математики і фізичних наук (IMSP), Республіка Бенін

² Фізичний факультет, Університет м. Абомей-Калаві, Республіка Бенін

³ Університет м. Наттінгу, Еколь нормаль сюпер'єр, Республіка Бенін

Досліджується змішана спин- $\frac{1}{2}$ і спин- $\frac{5}{2}$ модель на ґратці Бете в присутності магнітного поля h , використовуючи метод рекурсивних співвідношень. Побудована фазова діаграма основного стану, яка може бути використана для дослідження цікавих областей температурної фазової діаграми моделі. Для того, щоб прокласифікувати природу фазового переходу та отримати відповідні температури, детально досліджено параметри порядку, відповідні функції відгуку і внутрішню енергію. Так, при відсутності магнітного поля, температурні фазові діаграми є представлені для випадку однакового кристалічного поля на площині $(k_B T/|J|, D/|J|)$, коли $q = 3, 4, 5$ і 6 . Модель демонструє тільки фазовий перехід другого роду для відповідних значень фізичних параметрів моделі.

Ключові слова: магнітні системи, температурні зміни, фазові діаграми, магнітне поле, перехід другого роду
